Progress In Electromagnetics Research, Vol. 169, 103–115, 2020

Wideband RCS Reduction of High Gain Fabry-Perot Antenna Employing a Receiver-Transmitter Metasurface

Peng Xie, Guang-Ming Wang*, Hai-Peng Li, Ya-Wei Wang, and Binfeng Zong

Abstract—This paper presents a high gain Fabry-Perot antenna with radar cross section (RCS) reduction property. A receiver-transmitter metasurface is designed and used as the partially reflective surface (PRS) of the antenna to realize high gain and wideband RCS reduction. Firstly, the working principle of the unit cell is similar to the reception and radiation of two patch antennas. The unit cell is designed to present high reflectivity through tuning the impedance matching between two patches. This can ensure that the antenna obtains high gain. Then, the ground plane in the middle makes the reflection phase from different sides of the unit cell be tuned independently. Two unit cells with same reflection phase from the bottom side and 180° reflection phase difference from the top side are obtained through tuning the size of the transmitter patch. With the improved chessboard arrangement of these two unit cells, the incident wave can be scattered into many directions. So the metasurface presents a good RCS reduction property. More importantly, thanks to the high reflectivity of the metasurface, almost all the electromagnetic waves from the outside are reflected and rarely enter the cavity. Therefore, the antenna achieves good in band RCS reduction. The measured results of the fabricated antenna agree well with the simulated ones, which verify the correctness of the design. The antennas reaches the maximum gain of 18.2 dBi at 10 GHz. Wideband RCS reduction and good in band RCS reduction are also obtained by the antenna.

1. INTRODUCTION

With the development of modern wireless communication technology, the scattering characteristic of the communication equipment becomes more and more important. So, the radar cross section (RCS) reduction technology has become very important in both civil and military applications. As an important part in the communication system, the antenna is a main scattering source, due to the metal structure on its radiation aperture. So the RCS reduction of the antennas is a key technology for stealth platforms. Many researches have been carried out in low RCS antennas [1–8]. A method to reduce the RCS of a slot array antenna is proposed in [1]. A fishbone-shaped array is designed to make the antenna present the same amplitude and 180° phase difference for two cross-polarized reflected waves. So the RCS of the antenna is reduced. A low RCS stacked patch antenna using two-layer metasurface (MS) is presented in [2]. The upper layer metallic pattern is used to absorb incoming wave out of band, while the lower layer achieves in-band RCS reduction. In recent years, using metasurfaces to realize RCS reduction is an important research direction. Many methods have been investigated to reduce the RCS of MS [9–16]. Random combinatorial phase gradient metasurfaces is a common way to realize RCS reduction. An efficient method for designing broadband, wide-angle, and polarization independent diffusion MS for RCS reduction is proposed in [9]. The diffusion MS is constructed by collecting eight supercells with randomly distributed gradient directions. Then, the MS obtains a good RCS reduction performance. Besides, the chessboard arrangement is also an effective approach to realize

Received 27 June 2020, Accepted 30 December 2020, Scheduled 31 December 2020
* Corresponding author: Guang-Ming Wang (wgming01@sina.com).
The authors are with the Air and Missile Defense College, Air Force Engineering University, Xi'an, Shaanxi 710051, China.

RCS reduction. The chessboard MS with surface wave suppression is designed to obtain wideband RCS reduction in [10]. The −10 dB RCS reduction bandwidth of the upper frequency band is extended by the surface wave suppression of the unit cells.

Fabry-Perot cavity (FPC) antenna has attracted much attention due to its high gain and simple structure characteristics. With the metal structure on the antenna aperture, the FPC antenna presents large RCS. So the RCS reduction design of the FPC antenna is very necessary to promote the application of FPC antenna in stealth platforms. There are some researches on the low RCS FPC antenna [17–25]. A high gain and low-RCS FPC antenna is designed by employing a coding MS in [17]. The 2-bit coding MS with a random coding sequence can reduce the RCS of the antenna in a broadband. The proposed antenna realizes RCS reduction and keeps high gain simultaneously. In [18], two different frequency selection surface (FSS) units are used to form an MS for designing a low RCS FPC antenna. The RCS reduction is obtained due to the phase cancelation of the designed MS. A circularly polarized FPC antenna is designed in [19]. With the chessboard arranged polarization conversion MS, the antenna can also achieve RCS reduction property. In [20], a linear-to-circular polarization converter is designed to form a circularly polarized FPC antenna with low RCS. The bottom side of the converter is a partially reflective surface (PRS), and the top side is an absorbing surface (AS). The proposed antenna exhibits good circular polarization performance with RCS reduction property over a wide band.

For the purpose of obtaining high gain and low RCS simultaneously, a good idea is to design a metasurface with the property that the reflection phase from different sides can be controlled independently. So the receiver-transmitter metasurface is a good candidate [26]. A circularly polarized FPC antenna is designed in [26] employing a receiver-transmitter unit cell. However, in this work, the receiver-transmitter unit cell is used to realize RCS reduction of the FPC antenna.

In this paper, we design a low RCS MS based on a receiver-transmitter unit cell. Then, MS is used as the PRS of an FPC antenna to realize RCS reduction of the antenna. The unit cell adopts the conventional receiver-transmitter unit cell in our previous work [26]. This unit cell has the advantage of independently controlling the reflection phase from different sides. For the purpose of high gain and good radiation performance of the FPC antenna, the unit cell is designed to present high reflectivity firstly. Then, two unit cells with the same reflection phase from bottom side and 180° reflection phase difference from top side are designed by changing the size of the transmitter patches. Through arranging the two unit cells in an improvement chessboard pattern, make the MS realize wideband RCS reduction. A low RCS FPC antenna is formed by the proposed MS and a feeder antenna. The Fabry-Perot antenna obtains broadband RCS reduction while maintaining good radiation characteristics. Especially, good in-band RCS reduction is also obtained by the antenna due to the high reflectivity of the metasurface, because the electromagnetic waves from the outside are almost reflected and rarely enter the cavity.

The rest of the paper is organized as follows. In Section 2, a detail analysis of the FPC antenna is presented, including the resonance condition and estimation of the gain. The design procedure of the MS and FPC antenna is described in Section 3. Section 4 provides the radiation and scattering performance of the proposed antenna. The simulated and measured results of the fabricated antenna are also given. Finally, the conclusions are drawn in Section 5.

2. ANALYSIS OF THE ANTENNA

Fabry-Perot cavity antenna is a common kind of leaky wave antenna. It can obtain high gain properties with the help of the resonance cavity. The cavity is composed by the ground plane and a PRS. A radiator is set in the cavity to excite the antenna. The electromagnetic wave that resonates in the cavity will leak out through the PRS. When the wave coming out of the cavity is in phase, the antenna will realize high gain radiation. So the condition of the antenna resonance can be expressed as [27]:

$$\varphi_S + \varphi_D - \frac{4\pi h}{\lambda_0} = 2N\pi, \qquad N = 0, \pm 1, \pm 2 \ldots \tag{1}$$

λ_0 is the wavelength in free space. φ_S and φ_D represent reflection phase of PRS and ground plane, respectively. From the theoretical analysis in [27, 28]. The relationship between antenna directivity and the reflection magnitude of the PRS R can be expressed as:

$$D_r = 10 \log \frac{1+R}{1-R} \tag{2}$$

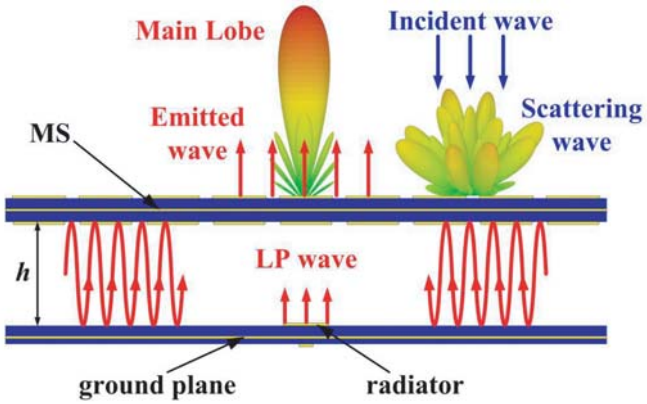

Figure 1. Sketch of the proposed low RCS FPC antenna.

It can be seen that the directivity of antenna is enhanced with the increase of R. Therefore, high reflectivity of PRS is necessary for obtaining high gain of the FPC antenna. In this paper, we replace the PRS with a well-designed MS to make the antenna achieve high gain and low RCS simultaneously. The sketch of the proposed FPC antenna is shown in Fig. 1.

3. DESIGN PROCESS OF THE ANTENNAS

3.1. Design of the Reference Antenna

Firstly, we design a reference antenna using a uniform MS. The unit cell of the MS is the conventional unit cell described in our previous work [26]. The configuration of the unit cell is shown in Figure 2. The substrate of the unit cell is the same as the unit cell in [26] (SCGA500-GF255, $\varepsilon_{r,sub} = 2.55$, $\tan\delta = 0.0014$, $h = 1.524\,\text{mm}$). The patch located on the bottom side of the lower substrate acts as the

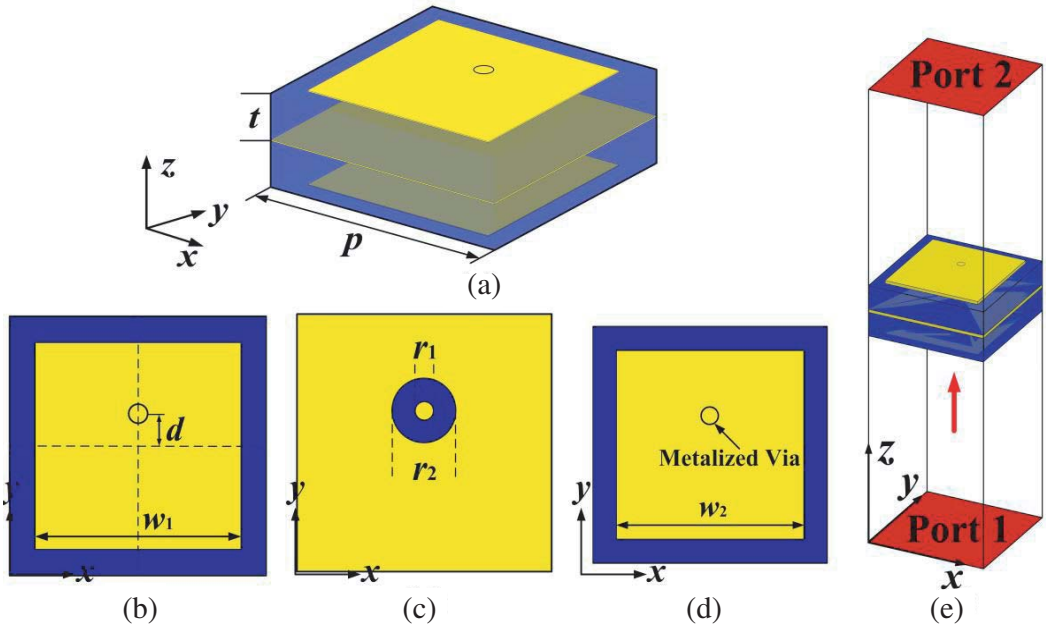

Figure 2. Structure of the unit cell. (a) Free view of the unit cell. Views of the (b) transmitter patch, (c) conducting ground, and (d) receiver patch. (e) Simulation model in the CST. ($p = 8\,\text{mm}$, $t = 1.524\,\text{mm}$, $r_1 = 0.6\,\text{mm}$, $r_2 = 1.6\,\text{mm}$, $w_2 = 6.46\,\text{mm}$).

receiver, and the patch located on the top side of the upper substrate acts as the transmitter. The two patches are connected by a metalized via-hole ($r_1 = 0.6\,\text{mm}$), which offsets the center with a distance of d in y-direction. The purpose of offsetting the metalized via-hole is to realize impedance matching between the receiver and transmitter patches. The views of the receiver and transmitter patches are shown in Figures 2(b) and (d), and Figure 2(c) is the view of the ground plane with a circular gap ($r_2 = 1.6\,\text{mm}$). In the simulation, unit cell boundary is set along x and y directions of the unit cell, while Floquet ports are set along z direction. The incident wave is first received by the receiver patch and coupled to the transmitter patch through the metalized via-hole. Then, the transmitter patch radiates circular polarization wave into the free space. In this design, the size of the unit cells is set as $8 \times 8\,\text{mm}^2$.

We know that the offset distance of the metalized via-hole d influences the impedance matching between radiator and transmitter patch. Then, the reflection and transmission magnitude of the unit cell can be tuned through varying d. The simulated reflection magnitude from bottom side of the unit cell varies with d, shown in Figure 3. The reflection magnitude of the unit cell goes up with the decrease of d. When d is reduced to 0.7 mm, the reflection magnitude of the unit cell reaches 0.93. The unit cell with $d = 0.7\,\text{mm}$ is named unit cell 0. The S parameters of the unit cell 0, including reflection magnitude, reflection phase, and transmission magnitude, are plotted in Figure 4. Using the unit cell 0, MS0 is formed. The MS0 consists of 16×16 unit cells, with a dimension of $128 \times 128\,\text{mm}^2$. The reference antenna is composed by the MS0 and a feeder. The view of the MS0 is shown in Figure 5(a). Unit cells at four corners of the MS are removed and replaced with four holes to facilitate the assembly of the antenna.

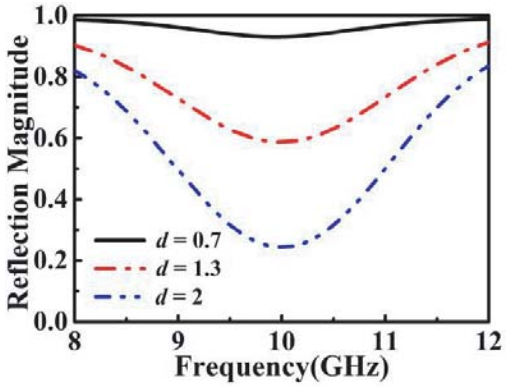

Figure 3. Simulated S_{11} of the unit cell varies with d.

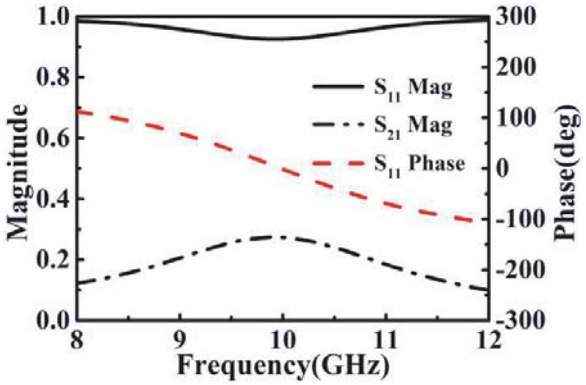

Figure 4. The S parameters of the unit cell with $d = 0.7\,\text{mm}$.

A slot coupled patch antenna is chosen as the feeder in our design due to its stable broadside radiation, as shown in Figure 5(b). The feed antenna consists of two substrates with identical material (SCGA500-GFF255, $\varepsilon_{r,sub} = 2.55$, $\tan\delta = 0.0014$) but different thicknesses ($h_u = 1.524\,\text{mm}$ and $h_b = 0.762\,\text{mm}$). Between two substrates is a ground plane with a slot under the radiation patch. The ground plane and MS form the FP resonant cavity. The radiation patch is printed on the top side of the upper substrate whereas the feeding line is printed on the bottom side of the lower substrate. A $50\,\Omega$ SMA connecter is used to feed the antenna from the edge of the substrate. Together with the feed antenna the reference antenna is formed. The height of the cavity h is obtained according to Eq. (1), which is set to 6.5 mm after optimization with the CST Microwave Studio. The reference antenna is named Antenna 0. The values of parameters of the Antenna 0 are displayed in Table 1.

3.2. Design of the Low RCS Antennas

To reduce the RCS of the FPC antenna, the MS used in the antenna should have a nonuniform reflection phase distribution from the top side (S_{22}). Meanwhile, to keep good resonance characteristics in the cavity, a uniform reflection phase distribution from the bottom side (S_{11}) of the MS is necessary. So we

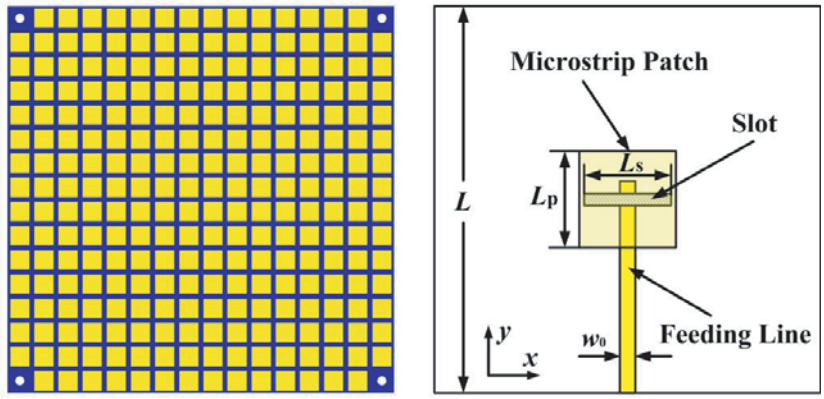

Figure 5. Configuration of (a) MS0 and (b) feed antenna. ($L_p = .6\,\text{mm}$, $L_s = 5.5\,\text{mm}$, $w_0 = 2.1\,\text{mm}$, $L = 128\,\text{mm}$).

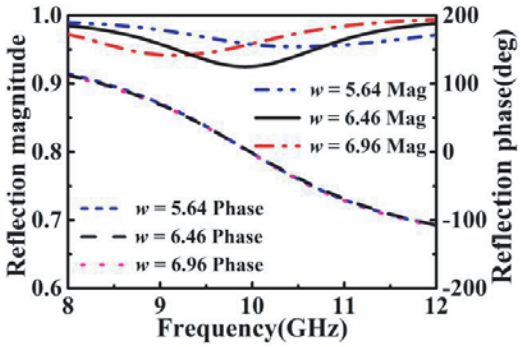

Figure 6. Simulated S_{11} of the unit cell varies with w_1.

Table 1. Parameters of the antenna.

Parameter	p	t	h	w_0	w_2	d
Value (mm)	8	1.524	6.5	2.1	6.46	0.7
Parameter	r_1	r_2	L	L_p	L_s	
Value (mm)	0.6	1.6	128	6.6	5.5	

improve the unit cell to present different phases of S_{22} without changing the phase of S_{11}. We find that changing the value of w_1 can only influence the phase of S_{22} and keep the phase of the S_{11} constant. The influence of w_1 on S_{11} is shown in Figure 6, and that on S_{22} is plotted in Figure 7. When w_1 goes up and goes down from 6.46 mm, respectively, the phase difference of S_{22} increases. When w_1 is set to 5.64 mm and 6.96 mm, the two unit cells have equal magnitudes and phases of S_{11} and 180° phase difference of S_{22} for both polarization waves. The unit cell with $w_1 = 5.64\,\text{mm}$ is named unit cell 1, and that with $w_1 = 6.96\,\text{mm}$ is named unit cell 2. The same S_{11} of unit cells can ensure good radiation characteristic of the antenna, and the 180° phase difference of S_{22} can be used to realize RCS reduction of the antenna. Figure 6(b) plots the phase of S_{21} of two unit cells. It can be found that S_{21} of two unit cells have 90° phase difference. This will influence the radiation performance and gain of the antenna. In order to overcome this disadvantage, it is preferred to arrange the same unit cells together on the MS. So the unit cell distribution of the MS is in chessboard arrangement, rather than random distribution or others. Besides, the reflection magnitudes of two unit cells are both very high.

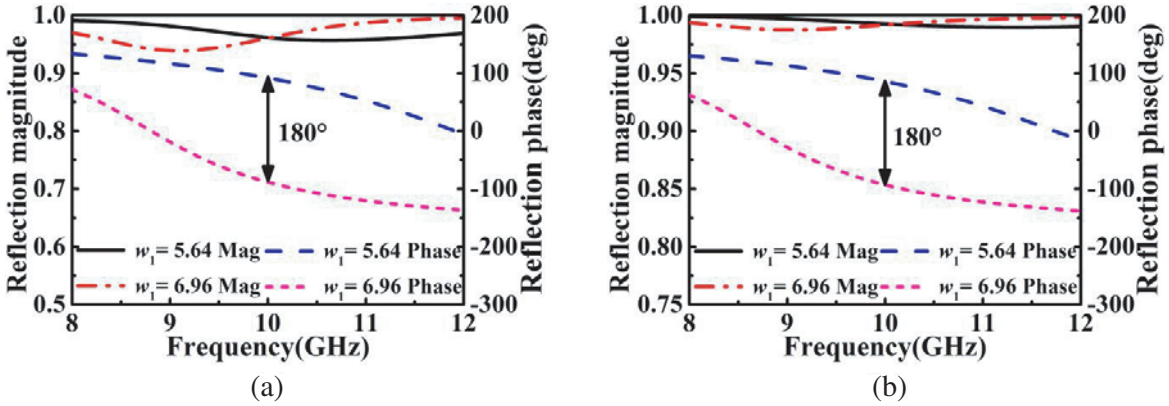

Figure 7. Simulated S_{22} of the unit cell under (a) y-polarization, and (b) x-polarization.

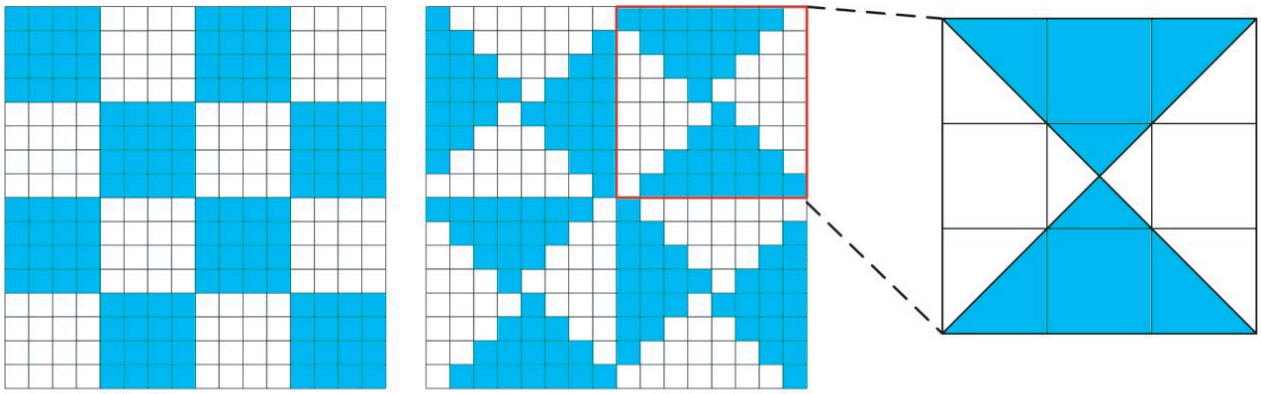

Figure 8. Two kinds of chessboard arrangement reflection phase distributions.

These properties can prevent the incident wave from entering the resonant cavity, so that the antenna can achieve good in-band RCS reduction.

The chessboard arrangement is a common method to realize RCS reduction [7, 8]. The MS adopts conventional chessboard arranged phase distribution, named MS1, as shown in Figure 8(a). Different colors represent unit cells with different phases of S_{22}. For the purpose of obtaining better RCS reduction performance, we propose an improved chessboard arranged method in this paper. The phase distribution of the new method is shown in Figure 8(b). The following simulation will show that this arrangement can make the MS have more scatter lobes to obtain better RCS reduction performance. The MS adopts the improved chessboard arranged phase distribution, named MS2. Figure 9 presents the top views of MSs. Together with the feed antenna shown in Figure 5(b), two low RCS FPC antennas named Antennas 1 and 2 are composed. The cavity heights of two antennas are the same as the reference antenna. Figure 10 shows the simulation model of antenna 2 in CST. The models of antenna 0 and antenna 1 are similar to antenna 2, so they are not given for simplicity.

The scattering field of the MS can be analyzed by array theory. Assuming that the unit cells on the MS have the same reflection magnitudes but different reflection phases, and the pattern of the scattering field is depended on the pattern of the array factor. The array factor of the unit cell (m, n) is expressed as:

$$f_{mn}(\theta,\varphi) = f_{xmn}(\theta,\varphi)\, f_{ymn}(\theta,\varphi)\, e^{j\varphi_{mn}} = e^{jmkx} e^{jnky} e^{j\varphi_{mn}} \tag{3}$$

where

$$x = d_x \sin\theta \cos\varphi \tag{4}$$

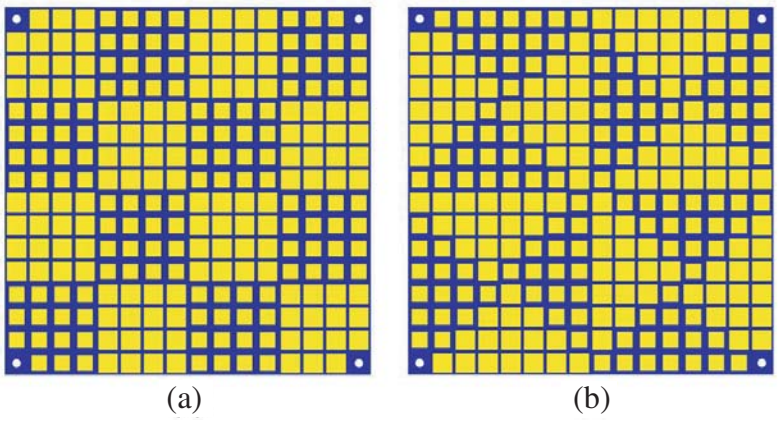

Figure 9. Configuration of (a) MS1 and (b) MS2.

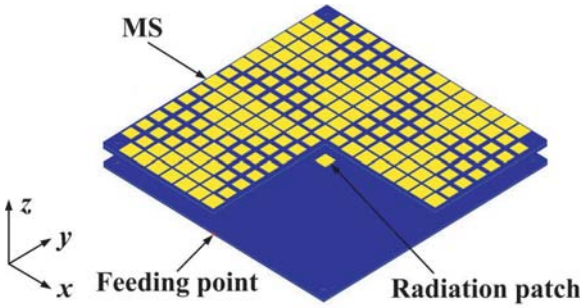

Figure 10. Structure of the proposed FPC antenna 2.

$$y = d_y \sin\theta \sin\varphi \tag{5}$$

φ_{mn} is the reflection phase of the unit cell. So the total array factor of the MS is:

$$f_{total} = \sum_{m=0}^{M-1}\sum_{n=0}^{N-1} f_{mn}(\theta,\varphi) = \sum_{m=0}^{M-1}\sum_{n=0}^{N-1} e^{jmkx} e^{jnky} e^{j\varphi_{mn}} \tag{6}$$

$e^{j\varphi_{mn}}$ of grids composed by unit cells with reflection phase of 0° and 180° are equal to 1 and −1, respectively. For the MS1, $e^{j\varphi_{mn}}$ can be expressed as:

$$e^{j\varphi_{mn}}_{\mathrm{MS1}} = \begin{bmatrix} 1 & -1 & 1 & -1 \\ -1 & 1 & -1 & 1 \\ 1 & -1 & 1 & -1 \\ -1 & 1 & -1 & 1 \end{bmatrix} \tag{7}$$

The reflection phase distribution of the MS2 can be equivalent to the figure shown in Figure 6(b). The grids that contain two kinds of unit cells have no contribution to the scattering field. $e^{j\varphi_{mn}}$ of these grids are deemed as 0. So $e^{j\varphi_{mn}}$ of MS2 can be expressed as:

$$e^{j\varphi_{mn}}_{\mathrm{MS2}} = \begin{bmatrix} 0 & 1 & 0 & 0 & -1 & 0 \\ -1 & 0 & -1 & 1 & 0 & 1 \\ 0 & 1 & 0 & 0 & -1 & 0 \\ 0 & -1 & 0 & 0 & 1 & 0 \\ 1 & 0 & 1 & -1 & 0 & -1 \\ 0 & -1 & 0 & 0 & 1 & 0 \end{bmatrix} \tag{8}$$

Then the scattering field of MS1 and MS2 can be obtained according to Equation (6). The calculated results show that the scattering field of MS1 has four grating lobes, and that of the MS2 has eight

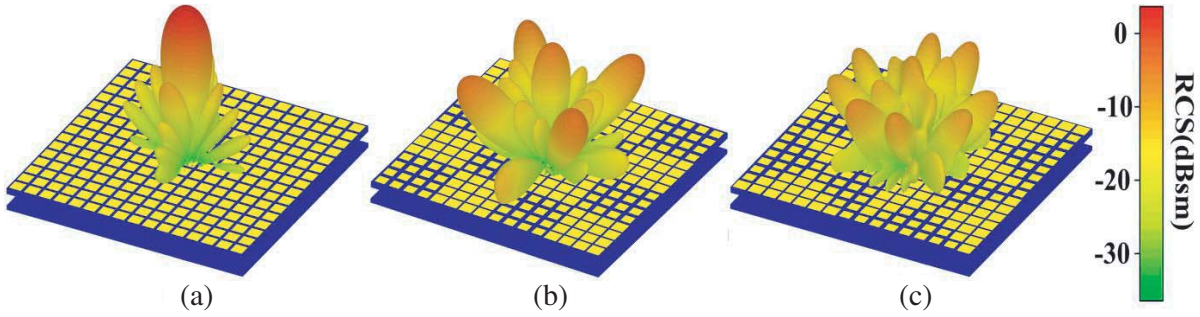

Figure 11. 3-D bistatic scattered field at 10 GHz under normal incidence for (a) antenna 0, (b) antenna 1, and (c) antenna 2.

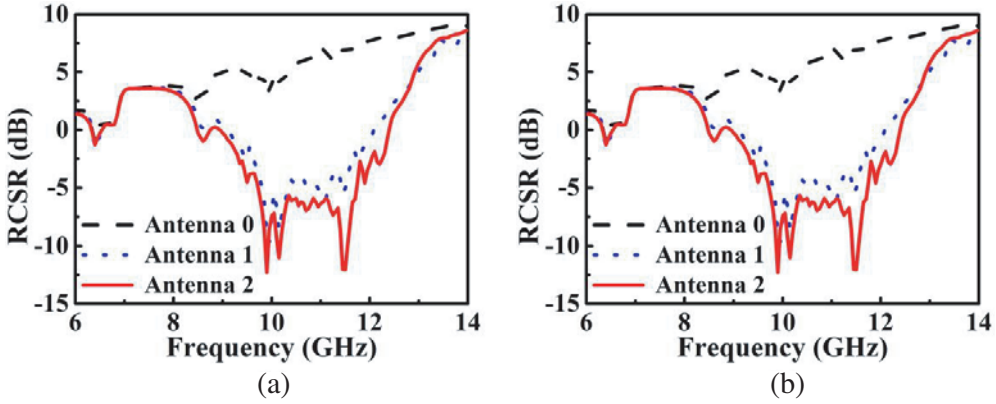

Figure 12. Monostatic RCS of antennas under (a) x-polarization and (b) y-polarization.

grating lobes. The improved arrangement can make the MS have more grating lobes to obtain better RCS reduction performance. This will be verified in the following simulation.

The RCS of antennas under normal incidence is simulated by the CST. The bistatic scattered fields of three antennas at 10 GHz are shown in Figure 11. With MS1, the scattered energy of antenna 1 is redistributed into five directions, and five grating lobes are obtained. However, the lobe in the normal direction is still large. The scattered energy of antenna 2 is dispersed into many different directions, forming many energy lobes. Furthermore, the monostatic RCSs of antennas with different polarization incident waves are shown in Figure 12. Figure 12(a) is the monostatic RCS of antennas with x-polarization incident wave, and Fig. 12(b) is that with y-polarization incident wave. We can see that RCS reduction performances are obtained by antennas 1 and 2, while antenna 2 has lower RCS than antenna 1 in the whole operating band. This shows that the improved chessboard arrangement has better RCS reduction performance than the traditional chessboard arrangement. So we adopt the improved chessboard arrangement to form the designed low RCS FPC antenna.

4. ANTENNA PERFORMANCE

4.1. Radiation Characteristics

The proposed FPC antenna 2 and reference antenna 0 are fabricated. The performance of the antennas is tested in an anechoic chamber. Figure 13 presents the measurement scene. Figure 14(a) plots the simulated and measured S_{11} of two antennas. The S_{11} of antenna 2 is similar to that of antenna 0. It shows that the two antennas have similar impedance matching conditions. This is because the reflection coefficients of MS2 are almost the same as that of MS0. The measured S_{11} of antenna 2 is lower than -10 dB in the band of 9.8–10.2 GHz. Besides, the application of the MS has little effect on the impedance

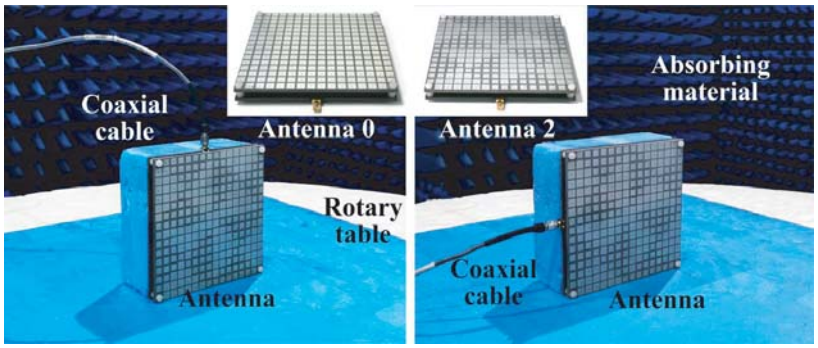

Figure 13. Measurement scene of fabricated antennas.

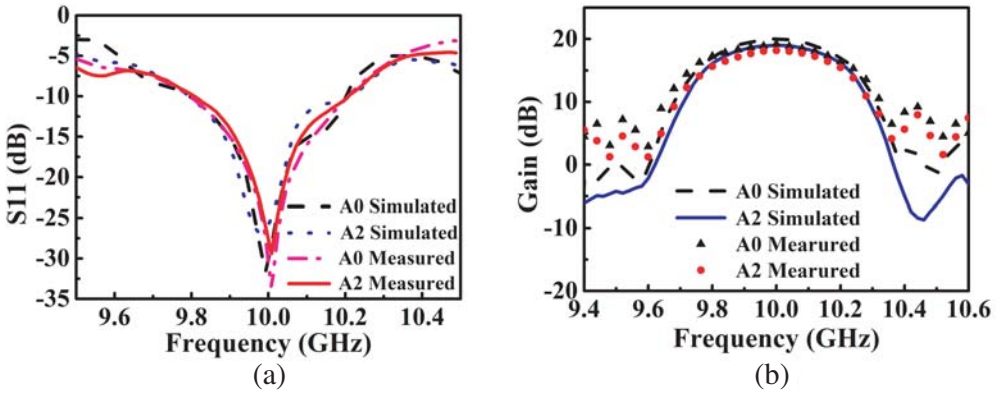

Figure 14. Performance of antennas. (a) S_{11}, and (b) gain.

of the feed antenna. So the impedance of the FPC antenna is similar to the feed antenna. The gains performances of two antennas are shown in Figure 14(b). The measured gains of antennas are all lower than simulated results. This may be caused by the fabricated errors and the energy loss introduced by the SMA connector. The maximum measured gain of antenna 2 (18.2 dBi) is lower than antenna 0 (19.1 dBi). This indicates that the chessboard arrangement of two unit cells has some influence on the gain of the antenna. Anyway, the designed antenna still maintains a high gain property. The aperture efficiency of the antenna is calculated according to:

$$\eta = G\frac{\lambda_0^2}{4\pi A} \tag{9}$$

The aperture efficiency of the proposed antenna is calculated as 28.9%.

As an important performance of the antenna, the radiation patterns of the antennas are measured in the anechoic chamber. The simulated and measured radiation patterns of the antenna are shown in Figure 15. Figures 15(a) and (b) show the patterns of antenna 0, and Figures 15(c) and (d) are the patterns of antenna 2. The measured results agree well with the simulated ones. The main beam of antenna 2 is almost unaffected by the chessboard arrangement, but more side lobes are obtained by antenna 2. This may be caused by the nonuniform sizes of radiator patches. However, the side lobe levels are all less than -20 dB. The cross-polarization levels of antenna 2 are less than -35 dB. The measured results show that antenna 2 presents good radiation patterns.

4.2. Scattering Performances

Horn antennas are employed as emitters and receivers to measure the scattering performances of two fabricated antennas. Matching loads are loaded to the antennas when the RCSs are tested. The

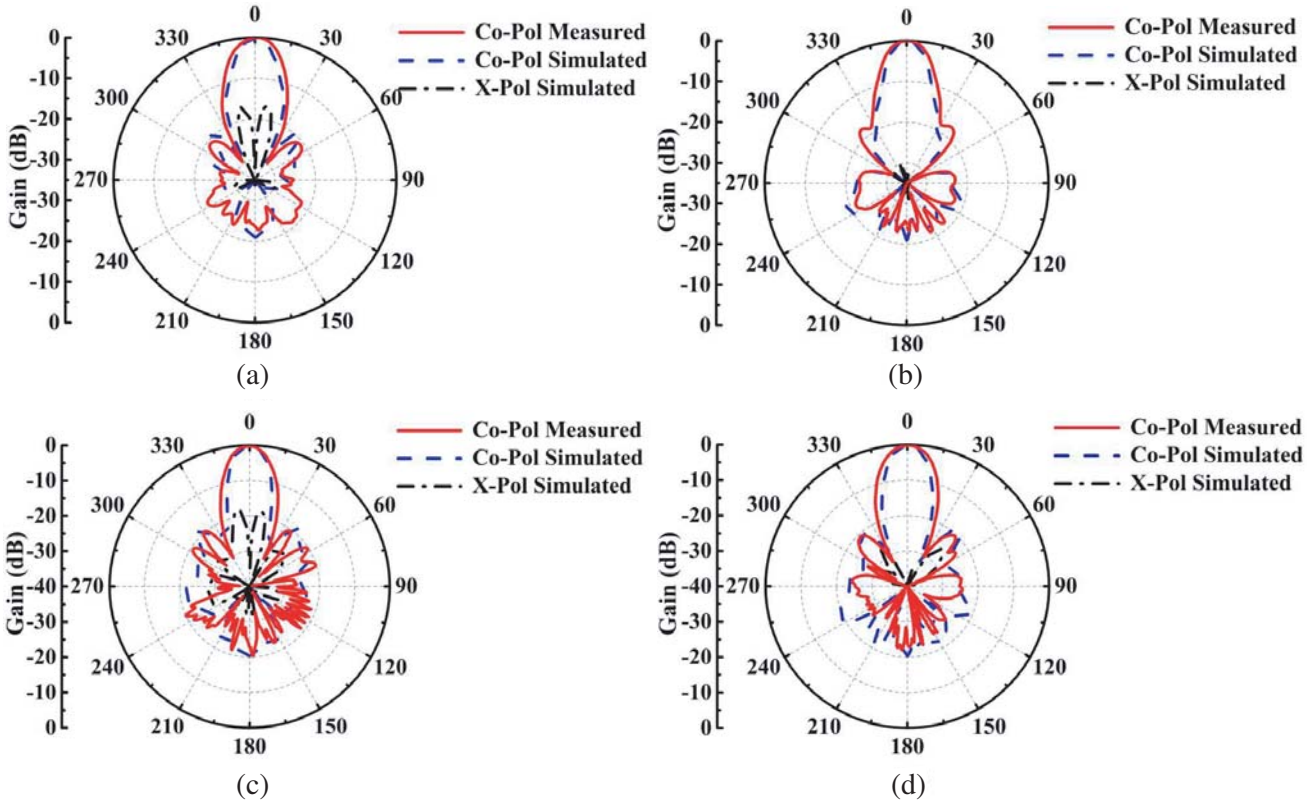

Figure 15. Radiation patterns of: (a) antenna 0 in *xoz* plane, (b) antenna 0 in *yoz* plane; (c) antenna 2 in *xoz* plane, and (d) antenna 2 in *yoz* plane.

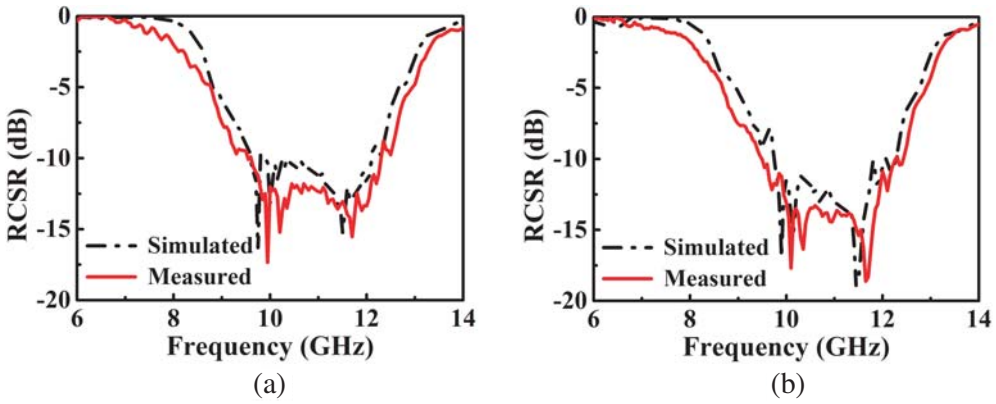

Figure 16. RCS reduction of antenna 2 under (a) x-polarization and (b) y-polarization.

measured RCS reduction (reference to antenna 0) of antenna 2 is shown in Figure 16. Figures 16(a) and (b) are the RCS reductions of the antenna 2 under x-polarization and y-polarization, respectively. Wideband RCS reduction is achieved by antenna 2 from 8 GHz to 14 GHz. The 10 dB RCS reduction is obtained from 9.5 GHz to 12.3 GHz, and the maximum RCS reduction reaches −18 dB. The RCS reduction of the antenna in the working band (9.8–10.2 GHz) is larger than 12.3 dB for both polarization waves, and good in-band RCS reduction is obtained by the proposed antenna 2. This is because the high reflectivity of the unit cell makes incident wave barely enter the resonant cavity.

To show the performance of the proposed low RCS FPC antenna more clearly, we give a comparison

Table 2. Comparison of low RCS FPC antennas.

Ref.	Gain (dBi)	Efficiency	Bandwidth (GHz)	Average RCS reduction	In band RCS reduction
[9]	19.8	55.5%	9.75–10.23	8.76 dB (8–12 GHz)	16.4 dB (TE) 3.8 dB (TM)
[10]	12	21.6%	9.42–11.35	10 dB (8–18 GHz)	15 dB (TE) 15 dB (TM)
[11]	11.2	32.4%	8.5–9.5	8 dB (6–16 GHz)	3 dB (TE) 4 dB (TM)
[12]	10.2	11.7%	10.5–10.75	10 dB (4–13 GHz)	7 dB (TE) 8 dB (TM)
proposed antenna	**18.2**	**28.9%**	**9.8–10.2**	**10 dB (8–14 GHz)**	**12.5 dB (TE) 12.3 dB (TM)**

between the proposed antenna and former reported antennas in Table 2. The operating band, peak gain, aperture efficiency, average RCS reduction, and in-band RCS reduction are all listed. From Table 2, we can observe that the maximum gain of the antenna reaches 18.2 dB at 10 GHz, and an average 10 dB RCS reduction is obtained by the antenna in the band of 8–14 GHz. Besides, the antenna exhibits good in-band RCS reduction property. Compared to other former reported antennas, the proposed antenna realizes high gain and wideband RCS reduction for both polarizations simultaneously, with good in-band RCS reduction.

5. CONCLUSION

In this paper, a receiver-transmitter MS for RCS reduction of FPC antenna is presented. The working principle of the unit cell adopted by the metasurface enables it to independently manipulate the reflection phase from different sides. The unit cell is designed to present high reflectivity first. Then, through tuning the size of the transmitter patch, two unit cells with same reflection phase from the bottom side and 180° reflection phase difference from the top side are obtained. Two unit cells are arranged in an improved chessboard pattern on the MS. The low RCS PFC antenna is composed by the proposed MS and a feed antenna. The performance of the designed antenna is verified by the measured results of the fabricated antenna. The antenna can realize wideband RCS reduction for both polarizations while maintain good radiation performance. Besides, the in-band RCS reduction is also very good due to the high reflectivity of the metasurface. Almost all the electromagnetic waves from the outside are reflected by the metasurface and rarely enter the cavity. Therefore, the antenna achieves good in band RCS reduction. The proposed low RCS antenna can be applied to many stealth communication systems.

ACKNOWLEDGMENT

This work was supported by the National Natural Foundation of China under Grant 61871394 and Natural Science Foundation of Shanxi Province under Grant 2018JQ6079.

REFERENCES

1. Liu, Y., K. Li, Y. Jia, Y. Hao, S. Gong, and Y. Jay Guo, "Wideband RCS reduction of a slot array antenna using polarization conversion metasurfaces," *IEEE Trans. Antennas Propag.*, Vol. 64, No. 1, 326–331, 2018.

2. Huang, C., W. Pan, X. Ma, and X. Luo, "Wideband radar cross section reduction of a stacked patch array antenna using metasurface," *IEEE Antennas Wireless Propag. Lett.*, Vol. 14, 1369–1372, 2015.
3. Krishnamoorthy, K., B. Majumder, J. Mukherjee, and K. P. Ray, "Low RCS and polarization reconfigurable antenna using cross slot based metasurface," *IEEE Antennas Wireless Propag. Lett.*, Vol. 14, 1638–1641, 2015.
4. Liu, Y., Y. Hao, K. Li, and S. Gong, "Wideband and polarization independent radar cross section reduction using holographic metasurface," *IEEE Antennas Wireless Propag. Lett.*, Vol. 15, 1028–1031, 2016.
5. Hong, T., S. Wang, Z. Liu, and S. Gong, "RCS reduction and gain enhancement for the circularly polarized array by polarization conversion metasurface coating," *IEEE Antennas Wireless Propag. Lett.*, Vol. 18, No. 1, 167–171, 2019.
6. Zhang, W., Y. Liu, S. Gong, J. Wang, and Y. Jiang, "Wideband RCS reduction of a slot array antenna using phase gradient metasurface," *IEEE Antennas Wireless Propag. Lett.*, Vol. 17, No. 12, 2193–2197, Dec. 2018.
7. Tran, X. L., J. Vesely, and F. Dvorak, "Optimization of nonuniform linear antenna array topology," *Information and Communication Technologies and Services*, Vol. 16, No. 3, 341–349, Sep. 2018.
8. Zakaria, Y. and L. Ivanek, "Propagation modelling of path loss models for wireless communication in urban and rural environments at 1800 GSM frequency band," *Information and Communication Technologies and Services*, Vol. 14, No. 2, 139–144, Jun. 2016.
9. Zhuang, Y., G. Wang, J. Liang, T. Cai, X. Tang, T. Guo, and Q. Zhang, "Random combinatorial gradient metasurface for broadband wide-angle and polarization independent difusion scattering," *Scientific Reports*, Vol. 7, 16560, Nov. 2017.
10. Kim, S. H. and Y. J. Yoon, "Wideband radar cross-section reduction on checkerboard metasurfaces with surface wave suppression," *IEEE IEEE Antennas Wireless Propag. Lett.*, Vol. 18, No. 5, 896–900, 2019.
11. Lu, Y., J. Su, J. Liu, Q. Guo, H. Yin, Z. Li, and J. Song, "Ultrawideband monostatic and bistatic RCS reductions for both copolarization and cross polarization based on polarization conversion and destructive interference," *IEEE Trans. Antennas Propag.*, Vol. 67, No. 7, 4936–4941, Jul. 2019.
12. Li, Y., J. Zhang, S. Qu, J. Wang, H. Chen, Z. Xu, and A. Zhang, "Wideband radar cross section reduction using two-dimensional phase gradient metasurfaces," *Appl. Phys. Lett.*, Vol. 104, 221110, 2014.
13. Zhuang, Y., G. Wang, T. Cai, and Q. Zhang, "Design of bifunctional metasurface based on independent control of transmission and reflection," *Optics Express*, Vol. 26, No. 3, 3594–3603, Feb. 2018.
14. Song, Y., J. Ding, C. Guo, Y. Ren, and J. Zhang, "Ultra broadband backscatter radar cross section reduction based on polarization insensitive metasurface," *IEEE Antennas Wireless Propag. Lett.*, Vol. 15, 329–331, 2016.
15. Joshi, A. and R. Singhal, "Vertex-fed hexagonal antenna with low cross-polarization levels," *Information and Communication Technologies and Services*, Vol. 17, No. 2, 138–145, Jun. 2019.
16. Mishra, B., V. Singh, and R. Singh, "Gap coupled dual-band petal shape patch antenna for WLAN/WiMAX applications," Vol. 16, No. 2, 185–198, Jun. 2018.
17. Zhang, L., X. Wan, S. Liu, J. Yin, Q. Zhang, H. Wu, and T. Cui, "Realization of low scattering for a high-gain Fabry-Perot antenna using coding metasurface," *IEEE Trans. Antennas Propag.*, Vol. 65, No. 7, 3374–3383, Jul. 2017.
18. Zheng, Y., J. Gao, Y. Zhou, X. Cao, H. Yang, S. Li, and T. Li, "Wideband gain enhancement and RCS reduction of Fabry-Perot resonator antenna with chessboard arranged metamaterial superstrate," *IEEE Trans. Antennas Propag.*, Vol. 66, No. 2, 590–599, Feb. 2018.
19. Li, K., Y. Liu, Y. Jia, and Y. J. Guo, "A circularly polarized high gain antenna with low RCS over a wideband using chessboard polarization conversion metasurfaces," *IEEE Trans. Antennas Propag.*, Vol. 65, No. 8, 4288–4292, Aug. 2017.

20. Ren, J., W. Jiang, K. Zhang, and S. Gong, "A high-gain circularly polarized fabry-perot antenna with wideband low-RCS property," *IEEE Antennas Wireless Propag. Lett.*, Vol. 17, No. 5, 853–856, May 2018.
21. Long, M., W. Jiang, and S. Gong, "Wideband RCS reduction using polarization conversion metasurface and partially reflecting surface," *IEEE Antennas Wireless Propag. Lett.*, Vol. 16, 2534–2537, 2017.
22. Zhou, Y., X. Cao, J. Gao, S. Li, and Y. Zheng, "In-band RCS reduction and gain enhancement of a dual-band PRMS-antenna," *IEEE Antennas Wireless Propag. Lett.*, Vol. 16, 2716–2720, 2017.
23. Zhang, L., C. Liu, C. Ni, M. Kong, and X. Wu, "Low-RCS, circular polarization, and high-gain broadband antenna based on mirror polarization conversion metasurfaces," *International Journal of Antennas and Propagation*, Vol. 2019, 6098483, Aug. 2019.
24. Ge, Y., Z. Sun, Z. Chen, and Y. Chen, "A high-gain wideband low-profile Fabry-Perot resonator antenna with a conical short horn," *IEEE Antennas Wireless Propag. Lett.*, Vol. 15, 1889–1892, 2016.
25. Sharmaa, A., D. Gangwarb, B. K. Kanaujiac, and S. Dwari, "Gain enhancement and RCS reduction of CP patch antenna using partially reflecting and absorbing metasurface," *Electromagnetics*, 2019.
26. Xie, P., G. Wang, H. Li, J. Liang, and X. Gao, "Circularly polarized Fabry-Perot antenna employing a receiver-transmitter polarization conversion metasurface," *IEEE Trans. Antennas Propag.*, Vol. 68, No. 4, 3213–3218, 2020.
27. Trentini, G. V., "Partially reflecting sheet arrays," *IEEE Trans. Antenna Propag.*, Vol. 4, No. 4, 666–671, Oct. 1956.
28. Foroozesh, A. and L. Shafai, "Investigation into the effects of the reflection phase characteristics of highly-reflective superstrates on resonant cavity antennas," *IEEE Trans. Antennas Propag.*, Vol. 58, 3392–3396, Oct. 2010.